HHS Public Access

Author manuscript

Mol Cancer Ther. Author manuscript; available in PMC 2018 December 01.

Published in final edited form as:

Mol Cancer Ther. 2017 December ; 16(12): 2881–2891. doi:10.1158/1535-7163.MCT-17-0587.

Inhibition of the Receptor Tyrosine Kinase AXL Restores Paclitaxel Chemosensitivity in Uterine Serous Cancer

Marguerite L. Palisoul[1,2,*], **Jeanne M. Quinn**[1,2,*], **Emily Schepers**[1,2], **Ian S. Hagemann**[3], **Lei Guo**[1,2], **Kelsey Reger**[1,2], **Andrea R. Hagemann**[1], **Carolyn K. McCourt**[1], **Premal H. Thaker**[1], **Matthew A. Powell**[1], **David G. Mutch**[1], and **Katherine C. Fuh**[1,2]

[1]Division of Gynecologic Oncology, Department of Obstetrics and Gynecology, Washington University School of Medicine, St. Louis, MO, USA

[2]Center for Reproductive Health Sciences, Washington University School of Medicine, St. Louis, MO, USA

[3]Department of Pathology and Immunology

Abstract

Uterine serous cancer (USC) is aggressive, and the majority of recurrent cases are chemoresistant. Because the receptor tyrosine kinase AXL promotes invasion and metastasis of USC and is implicated in chemoresistance in other cancers, we assessed the role of AXL in paclitaxel resistance in USC, determined the mechanism of action, and sought to restore chemosensitivity by inhibiting AXL *in vitro* and *in vivo*. We used small hairpin RNAs and BGB324 to knock down and inhibit AXL. We assessed sensitivity of USC cell lines to paclitaxel and measured paclitaxel intracellular accumulation *in vitro* in the presence or absence of AXL. We also examined the role of the epithelial-mesenchymal transition in AXL-mediated paclitaxel resistance. Finally, we treated USC xenografts with paclitaxel, BGB324, or paclitaxel plus BGB324 and monitored tumor burden. AXL expression was higher in chemoresistant USC patient tumors and cell lines than in chemosensitive tumors and cell lines. Knockdown or inhibition of AXL increased sensitivity of USC cell lines to paclitaxel *in vitro* and increased cellular accumulation of paclitaxel. AXL promoted chemoresistance even in cells that underwent the epithelial-mesenchymal transition *in vitro*. Finally, *in vivo* studies of combination treatment with BGB324 and paclitaxel showed a greater than 51% decrease in tumor volume after 2 weeks of treatment when compared to no treatment or single agent treatments ($P<0.001$). Our results show that AXL expression mediates chemoresistance independent of EMT and prevents accumulation of paclitaxel. This study supports the continued investigation of AXL as a clinical target, particularly in chemoresistant USC.

Keywords

Epithelial mesenchymal transition; BGB324; R428; paclitaxel retention; apoptosis; xenograft mouse model; TCGA

Corresponding Author: Katherine C. Fuh, MD, PhD, 425 So. Euclid Avenue, Box 8064, St. Louis, MO 63110, Ph: 314-362-8155, Fax: 314-362-2893, kfuh@wudosis.wustl.edu.

*Denotes authors had equal contribution

2. Introduction

Endometrial cancer is the most common gynecologic malignancy in the United States, and the incidence and attributed death rates are rising. There will be an estimated 61,380 new cases diagnosed in the year 2017 [1]. Of these, 10% will be uterine serous carcinoma (USC), which is more aggressive and difficult to treat than other histologies [2] and is responsible for up to 40% of deaths from uterine cancer each year [3]. Currently, USC patients are treated with platinum and taxane, to which 50-60% of tumors respond. However, 40-50% of USC tumors are resistant to chemotherapy [4, 5]. Thus, defining the pathways involved in USC chemoresistance will be important to improve outcomes for these patients.

In recent work, we demonstrated that advanced stage and high-grade uterine cancer specimens expressed high levels of the receptor tyrosine kinase AXL and that AXL expression correlated with poor survival. Additionally, we found that AXL was required for migration and invasion of the USC cell line ARK1 *in vitro* and that ARK1 cells in which AXL was knocked down produced smaller tumor burden than AXL-expressing cells in a metastatic xenograft model [6]. These data were consistent with findings that AXL is a critical player in the metastatic potential and overall prognosis of numerous other solid cancers [7-11]. Binding of AXL to its only ligand, growth arrest specific gene-6 (GAS6), induces proliferation, survival, invasion, metastasis, avoidance of apoptosis, and angiogenesis in other tumor types [12, 13], though no activating mutation has been identified in AXL [14]. AXL acts through a number of downstream pathways, including the PI3K/AKT and Ras/ERK pathways [15].

Several lines of evidence indicate that AXL plays a role in chemoresistance in other tumors. For example, increased AXL expression was observed in non-small cell lung cancers with activating mutations in epidermal growth factor receptor (EGFR) that acquired resistance to the EGFR inhibitor erlotinib. Furthermore, genetic or pharmacological inhibition of AXL prevented or overcame the acquired resistance in these tumors [16-19]. AXL appears to promote resistance by several mechanisms, including feedback loops and receptor crosstalk in signaling pathways, cell survival and anti-apoptotic mechanisms, and alterations in the tumor microenvironment [18, 20-26]. In addition, AXL can regulate the epithelial-mesenchymal transition (EMT) and EMT can influence AXL expression, thus contributing to invasive and chemoresistant phenotypes [16, 27-31].

Given these findings that AXL promotes chemoresistance in other cancers and our findings that AXL is required for uterine cancer cell migration, invasion, and metastasis [6], our objective here was to assess the role of AXL in chemoresistance in USC. We report that AXL expression mediates USC resistance to paclitaxel-induced cell cycle arrest and apoptosis independently of EMT. Moreover, we demonstrate that inhibition of AXL restores USC chemosensitivity and thus may provide a therapeutic strategy for chemoresistant uterine cancer.

3. Materials and Methods

3.1. TCGA Oncoprint

The Uterine Corpus Endometrial Carcinoma dataset from The Cancer Genome Atlas was accessed through www.cbioportal.org to develop an Oncoprint. The published dataset included 240 uterine cancer tumors with copy number alterations data. Limited clinical information was available including disease status [32, 33].

3.2. Clinical samples and immunohistochemistry

A tissue microarray containing specimens from primary and metastatic uterine serous carcinoma was developed under IRB approval #201409005 from patients treated at Washington University in St Louis. Written informed consent was obtained for tumor banking, and specimens were obtained in accordance with recognized ethical guidelines per the U.S. Common Rule. Patients were considered chemoresistant if disease recurred within 6 months of last chemotherapy regimen. Briefly, slides were deparaffinized with xylene, rehydrated according to standard methods, and stained with anti-AXL primary antibody (R&D Systems, Minneapolis, MN). Two cores per patient were evaluated by a similar system developed and validated by Rankin and colleagues [9]. Intensity based on degree of brown staining and percentage of positive immunoreactive cells were blindly scored by two independent reviewers, averaged, stratified, and assigned a corresponding histology score (0 for 0-15%, 1 for 16-40%, 2 for 41-70%, and 3 for 71-100%).

3.3. Cell Lines and Culture Conditions

Established human, immortalized, previously characterized USC cell lines were used [34, 35]. ARK1 cells were provided by Shi-Wen Jiang (Mercer University School of Medicine, Savannah, GA) in 2010, ARK4 cells were purchased from Dr. A. Santin (Yale University, New Haven, CT) in 2016, and AN3CA cells were provided by Yan Yin (Washington University School of Medicine, St. Louis, MO) in 2010. ARK1 and ARK4 cells were cultured in RPMI (Sigma-Aldrich, St. Louis, MO) supplemented with 10% heat-inactivated fetal bovine serum (FBS) (Sigma-Aldrich) and 1% penicillin and streptomycin (ThermoFisher, Waltham, MA). AN3CA cells were cultured in DMEM (Sigma-Aldrich) similarly supplemented with FBS and antibiotic. The AXL ligand GAS6 (R&D Systems, Minneapolis, MN) was used to stimulate AXL phosphorylation. To induce mesenchymal phenotypes, cells were cultured with 100 ng/mL TGFβ (Peprotech, Rocky Hill, NJ) and 50 ng/mL TNFα (R&D systems) for at least seven days. All cells were maintained at 37°C in a 5% CO_2 incubator. Cell lines were authenticated by IDEXX Bioresearch, which performs short tandem repeat profile and interspecies contamination testing. All cell lines were confirmed negative for mycoplasma, as indicated by the MycoAlert Mycoplasma Detection Kit (Lonza, Basel, Switzerland), before performing experiments and re-tested before subsequent experiments.

3.4. Stable transfection with short hairpin RNA to knock down AXL expression

Oligos encoding an AXL shRNA (shAXL-S) were synthesized as previously described [36] (5′-GATTTGGAGAACACACTGA-3′), and an additional shAXL-C4 construct was

similarly synthesized (5′-GCTGTGAAGACGATGAAGATT-3′). A scrambled sequence was used as a non-targeting shRNA control (5′-AATTGTACTACACAAAAGTAC-3′). shSCRM-S and shAXL-S oligos were cloned into the pSiren RetroQ vector (BD Biosciences, Franklin Lakes, NJ), and viral particles were produced in 293T cells. Target cells were incubated with viral media for 24 h. shAXL-C4 oligos were cloned into p156 RRL-hTERT vector plasmid, and viral media was incubated with target cells for 4 h. Cells were then selected in puromycin (Sigma-Aldrich), and AXL knockdown in polyclonal cell populations was validated by Western blot.

3.5. Western blot analysis

Protein lysates were harvested in 9 M Urea, 0.075 M Tris buffer (pH 7.6). Protein lysates were quantified by using the Bradford assay and subjected to reducing SDS-PAGE according to standard methods. Western blots were probed with antibodies against AXL (1:1000, R&D Systems), β-actin (1:1000, Sigma-Aldrich), p-AXL702/703 (1:500, Cell Signaling), AKT (1:1000, Cell Signaling), PARP (1:500, Santa Cruz Biotechnology, Dallas, TX), E-cadherin (1:1000, Cell Signaling), Vimentin (1:1000, BD Biosciences), and Slug (1:1000, BD Biosciences). Appropriate horseradish peroxidase-conjugated secondary antibodies were used (Jackson ImmunoResearch, West Grove, PA), and chemiluminescence was measured on a ChemiDoc (Bio-Rad Laboratories, Hercules, CA).

3.6. Drug treatment and cell growth (XTT) assays

For cell growth assays, 5×10^3 cells were plated in each well of a 96-well plate. The cells were allowed to attach overnight, then vehicle or drug was added to each well. Cells were treated with paclitaxel (Sigma-Aldrich) in increasing concentrations from 0.7 nM to 320 nM. When using the small molecule inhibitor of AXL, BGB324 (also known as R428) (Selleckchem) [37], cells were pre-treated with BGB324 for 4 hours, then treated with a combination of paclitaxel and BGB324. After 72 hours, a 2,3-bis(2-methoxy-4-nitro-5-sulfophenyl)-2*H*-tetrazolium-5-carboxanilide inner salt (XTT)-based assay (Sigma-Aldrich) was performed as previously described [37] to measure viability. The 96-well plates were returned to the 37°C incubator for 1 to 2 hours. Metabolism of XTT was quantified by measuring the absorbance at 450 nm (Tecan infinite M200 Pro). Experimental data were quantified relative to values obtained for the control cells.

3.7. Clonal survival assay

Cells were plated in duplicate at a density of 500 cells per well in standard 6-well tissue culture plates and allowed to attach overnight. Then, vehicle or drug was added to the dishes, and cells were incubated in the presence of drug for 7 days. At the conclusion of the incubation period, colonies were identified with crystal violet stain (6.0% glutaraldehyde + 0.5% crystal violet), and plating efficiency and surviving fraction were calculated.

3.8. Cell cycle analysis

Cells were plated at a density of 5×10^5 cells per 10 cm dish and allowed to attach overnight. The day after plating, vehicle or drug (10 nM paclitaxel) was added to each plate and incubated for 6 h. Cells were harvested and combined with the culture supernatants, then

fixed with 90% ethanol for 30 min at 4°C. Fixed cells were pelleted, resuspended in PBS, and incubated with 50 μg/mL RNAse for 1 h at 37°C. Then, cells were pelleted, resuspended in PBS, and stained with 100 μg/mL propidium iodide (PI) for 1 h at 37°C. Fluorescense was measured by flow cytometry on a FACSCalibur flow cytometer (BD Biosciences), and cell cycle was fit with FlowJo software.

3.9. Flow cytometry assessment of apoptosis

The Annexin-V/PI kit (eBioscience, San Diego, CA) was used. Cells were plated at a density of 2×10^5 cells per 10 cm dish and allowed to attach overnight. The day after plating, vehicle or drug was added to each plate and incubated for 24 h. Cells were harvested and combined with the culture supernatants. Cell pellets were washed with PBS then 1X Binding Buffer, then were resuspended in 1X Binding Buffer at 1-5 × 10^6 cells/mL; 5 μL of fluorochrome-conjugated Annexin V was added to 100 μL of the cell suspension and incubated for 15 min at room temperature, protected from light. The cells were then washed with 1X Binding Buffer and resuspended in 200 μL of 1X Binding Buffer. Next, cells were stained with 5 μL PI Staining Solution and analyzed by flow cytometry within 4 hours on a FACSCalibur flow cytometer (BD Biosciences). Apoptotic cells were quantified with FlowJo software.

3.10. Assessment of apoptotic nuclei

Cells were plated at a density of 1.6×10^5 cells per well in 6-well plates and allowed to attach overnight. Then, vehicle or drug was added to the plate and incubated for 24 h. Cells were fixed and permeabilized in 4% paraformaldehyde (ThermoFisher) and 0.1% Triton-X 100 (Sigma-Aldrich) in cold PBS. Mounting media containing 6-diamiidino-2-phenylindole (DAPI) (Vector Laboratories, Burlingame, CA) was applied to fixed cells, and nuclear morphology was assessed by fluorescent microscopy.

3.11. Measurement of paclitaxel accumulation

Cells were plated at a density of 5×10^5 cells per 10 cm dish and allowed to attach overnight. For experiments with shAXL- and shSCRM-treated cells, cells were then incubated with 10 nM [H^3]paclitaxel (100 pmol) (Movarek, Brea, CA) or vehicle control for 2 h. For experiments with BGB324, cells were first pre-treated with BGB324 for 2 h, then treated with [H^3]paclitaxel as above. Media was removed, cells were washed three times with PBS, and lysates were collected. To measure remaining intracellular paclitaxel post-treatment, cells were removed from [H^3]paclitaxel supplemented media, washed, and incubated in fresh media for 2 or 4 h before lysate preparation. Samples were added to scintillation fluid and analyzed in a liquid scintillation counter (Beckman Coulter, Pasadena, CA).

3.12. cDNA preparation and quantitative real time PCR

The RNEasy mini kit (Qiagen, Hilden, Germany) was used to isolate total RNA from cells, 1 ug of which was used to make cDNA using the SuperScript IV system (ThermoFisher) according to the manufacturer's directions. Applied Biosystems 7500 detection system and SYBR-green master mix (ThermoFisher) were used to perform quantitative PCR (qPCR). mRNA expression was normalized with respect to glyceraldehyde-3-phosphate

dehydrogenase. Fold change was calculated using the 2(x0005E)(-ΔΔCT) method. Primer sequences were previously published [9, 38, 39].

3.13. Tumor xenograft model

Female (NOD) SCID mice (Jackson Laboratory) aged 6-8 weeks were used to establish tumor xenograft models. Experiments were conducted according to institutional animal care and use committee (IACUC) policy. ARK1shSCRM cells (1×10^7) were resuspended in 1 mg/mL Matrigel (Corning, Corning, NY) and injected subcutaneously onto the flank. After tumor engraftment, tumors were measured every three days with calipers and tumor volume was calculated using the equation V=l*w*π/6 (l=longest diameter, w=shortest, perpendicular diameter). Relative tumor volume for control and treatment conditions (V_C or V_T was calculated by normalizing tumor volume at day 14 over tumor volume at day 1. Relative tumor growth (V_T / V_C) was then calculated for each treatment condition.

3.14. Statistical analysis

Data are shown as representative example of at least three independent experiments. Statistical analyses and IC_{50} calculations were performed using GraphPad Prism 7. Statistical significance between groups was determined by unpaired t-tests and defined as $P<0.05$.

4. Results

4.1. AXL expression is elevated in chemoresistant USC patient tumors

Given our previous observation that AXL expression correlated with poor survival in endometrial cancer patients, we wondered whether AXL expression also correlated with response to treatment. First, we queried data from The Cancer Genome Atlas project and identified 43 USCs with information on copy number alterations. We found that two of the patients had AXL gene amplification, and both of these patients' cancers had recurred (Fig. S1) [40]. Next, we examined AXL expression by immunohistochemistry in a panel of 82 USC tumors from patients treated with chemotherapy at Washington University. We scored the level of AXL expression on a scale from 0 to 3 and found that chemoresistant tumors had a significantly higher mean score than did those from chemosensitive and non-recurrent cases (Table 1 and Fig. S2).

4.2. Increased AXL expression is associated with resistance to paclitaxel in USC

To determine whether AXL expression correlates with chemotherapy response in USC, we first evaluated expression of AXL protein in three cell lines, ARK1, ARK4, and AN3CA. The cell line AN3CA was derived from a chemosensitive uterine adenocarcinoma, whereas ARK1 and ARK4 were derived from chemoresistant pure USC. As shown in Fig. 1A, AXL expression was markedly higher in ARK1 and ARK4 cells than in AN3CA cells. We then compared the effects of paclitaxel chemotherapy between these three cell lines. The AXL-expressing cell lines, ARK1 and ARK4, were more resistant to paclitaxel than the AXL-non-expressing cell line, AN3CA (Fig. 1B). The IC_{50} values for paclitaxel were 4.4- and 3.0-fold higher in ARK1 and ARK4 cells, respectively, than in AN3CA cells. These results indicate that AXL expression correlates with paclitaxel resistance.

4.3. Knockdown of AXL expression enhances USC sensitivity to paclitaxel

To determine whether AXL is required for paclitaxel resistance in USC cell lines, we used lentiviruses to deliver AXL-specific shRNA constructs (shAXL-S and shAXL-C4) or a scrambled sequence (shSCRM) to ARK1 and ARK4 cells. After confirming by Western blot that AXL expression was reduced (Fig. 1C), we treated the cells with vehicle or 0.7 nM to 320 nM paclitaxel for 72 hours, and then assessed viability via the XTT assay. Cells in which AXL was knocked down were significantly more sensitive to paclitaxel (with 31–75% lower IC_{50} values) than the parent AXL-expressing cell lines (Fig. 1D). Consistent with our XTT assay results, we also found that ARK1 cells containing the shAXL-S construct had significantly lower clonogenicity than cells containing the shSCRM construct (Fig. S3).

4.4. Inhibition of AXL with BGB324 enhances USC sensitivity to paclitaxel

Next, we asked whether inhibiting AXL with the tyrosine kinase inhibitor BGB324 (also called R428) [37] would similarly increase USC cells' sensitivity to paclitaxel. First, to confirm that BGB324 inhibited AXL activation in a dose-dependent manner, we treated ARK1 cells with vehicle or BGB324 in the presence of the AXL-specific ligand GAS6, which induces AXL phosphorylation. As expected, BGB324 inhibited GAS6-induced AXL phosphorylation in a dose-dependent manner (Fig. 1E). Next, we pre-treated ARK1 or ARK4 cells with BGB324 for 4 hours, then added increasing concentrations of paclitaxel and measured viability 72 hours later. Treatment with BGB324 increased chemosensitivity in both ARK1 and ARK4 cell lines in a dose-dependent manner (Fig. 1F). Importantly, treatment with increasing concentrations of BGB324 alone had no effect on cell viability (Fig. S4). Additionally, Settleman and colleagues demonstrate that at the same 1μM dose of BGB324, AXL-null cells did not show reduction in invasion, migration, or chemoresponse [16]. Taken together, these data demonstrate that inhibition or knockdown of AXL restores sensitivity to paclitaxel in USC.

4.5. AXL expression reduces paclitaxel-induced cell cycle arrest and apoptosis

We next sought to determine the mechanism by which AXL inhibition improves paclitaxel sensitivity in USC cells (Fig. 2A). Because paclitaxel stabilizes microtubules, leading to cell cycle arrest and apoptosis [41], we first examined the effect of AXL inhibition on the cell cycle. Flow cytometry revealed that loss of AXL had little effect on the percentage of vehicle-exposed cells in the G2/M phase (29.8%, vs 26.1%). However, loss of AXL in paclitaxel-treated cells significantly increased the percentage of cells in the G2/M phase (33.9% vs 42.9%, $P<0.05$).

We assessed the effect of loss of AXL on paclitaxel-induced apoptosis in three ways. First, we used the Annexin-V/PI method to detect apoptotic cells by flow cytometry. At each paclitaxel concentration tested, ARK1 cells in which AXL was knocked down with shAXL had higher levels of apoptosis than the shSCRM-treated cells (Fig. 2B, S5). To confirm that the observed differences in apoptosis were specific to paclitaxel and not due to stress or differences in cell fitness, we serum starved the two groups of ARK1 cells and found that fewer than 3% of shAXL- or shSCRM-treated cells were apoptotic (Fig. S5).

Second, we confirmed differences in the magnitude of apoptosis between ARK1shSCRM and ARK1shAXL-S cells by visually examining nuclear morphology after treating cells with paclitaxel for 24 hours. We found that features associated with apoptosis including abnormal DNA condensation (arrowhead) and nuclear blebbing (arrow) were more common in shAXL-treated ARK1 cells than in shSCRM-treated ARK1 cells (Fig. 2C, 2D, S5).

Finally, we performed Western blots to assess the level of the apoptosis marker cleaved PARP in ARK1 cells. In the presence of paclitaxel, ARK1shAXL-S cells contained more cleaved PARP than did ARK1shSCRM cells (Fig. 2E). Similarly, ARK1 cells treated with BGB324 contained more cleaved PARP in the presence of paclitaxel than did cells not treated with the AXL inhibitor (Fig. 2F). Collectively, these three methods indicate that the AXL-expressing cells are less sensitive to paclitaxel-induced cell cycle arrest and apoptosis than AXL-non-expressing cells.

4.6. AXL inhibition increases intracellular paclitaxel accumulation

Given these findings, we wondered whether AXL expression affected accumulation of paclitaxel in cells. Thus, we treated ARK1shSCRM and ARK1shAXL cells with [^{3}H]paclitaxel for two hours and then quantitated the accumulated paclitaxel. ARK1shAXL cells contained 54% more intracellular paclitaxel than did ARK1shSCRM cells (Fig. 3A). Similarly, cells treated with 0.5 μM or 1 μM BGB324 contained 31% or 43% more paclitaxel, respectively, than cells treated with vehicle control (Fig. 3B). The higher amount of paclitaxel in BGB324-treated cells could indicate that they take up more paclitaxel than untreated cells or that they secrete paclitaxel more slowly. To assess this, we measured the amount of [^{3}H]paclitaxel in cells after two- and four-hour washout periods. We found no significant difference in intracellular paclitaxel at the time points measured (Fig. 3C), suggesting that cells in which AXL is active accumulate less paclitaxel than do cells in which AXL is inhibited. Additionally, we investigated whether cells with genetically inactivated AXL demonstrated differences in RNA corresponding to known multidrug resistant proteins (Fig. 3D). In agreement with Lin and colleagues' findings that AXL-expressing cells show increased pGP (ABCB1) mRNA [25], ARK1 cells transfected with shAXL RNA demonstrated downregulated pGP mRNA when compared to shSCRM-transfected cells.

4.7. AXL expression is positively associated with mesenchymal and chemoresistant phenotypes

To metastasize, uterine cancer cells undergo EMT, and mesenchymal cells are often more resistant to chemotherapy than are epithelial cells. Thus, we wondered whether AXL-expressing cells were chemoresistant because of their mesenchymal phenotype. To test this, we first confirmed by Western blot that ARK1 and ARK4 cells, which express AXL, expressed higher levels of the mesenchymal markers vimentin and slug and lower levels of the epithelial marker E-cadherin than AN3CA cells, which do not express AXL (Fig. 4A). To determine whether AXL was required for the mesenchymal phenotype in USC cells, we compared expression of mesenchymal and epithelial markers in ARK1shSCRM and ARK1shAXL-S cells and found that cells expressing AXL expressed more vimentin and less E-cadherin than cells in which AXL expression was knocked down (Fig. 4B).

If the mesenchymal phenotype is sufficient for paclitaxel resistance, then epithelial cells that are induced to undergo EMT should be paclitaxel resistant. To test this, we treated AN3CA cells with TGFβ and TNFα. These cells underwent EMT as evidenced by increased expression of vimentin, slug, and AXL and decreased expression of E-cadherin (Fig. 4C). We then compared paclitaxel sensitivity in AN3CA cells that had vs. those that had not undergone EMT and found that treated, “mesenchymal” AN3CA cells were more resistant to paclitaxel than untreated, “epithelial” AN3CA cells (Fig. 4D).

The preceding experiment indicated that the mesenchymal phenotype, which included AXL expression, was sufficient for paclitaxel resistance. To independently interrogate the role for mesenchymal phenotype vs. AXL expression in chemoresponse, we used shRNAs to knock down AXL expression in AN3CA cells and then treated them with TGFβ and TNFα to induce EMT (Fig. S6). We first confirmed that both shAXL- and shSCRM-treated AN3CA cells could be induced to take on a mesenchymal phenotype as evidenced by increased expression of vimentin and slug and decreased expression of E-cadherin (Fig. 4E). While the decrease in ECAD is less dramatic in the transfected cells, this could be due to the short treatment period for EMT induction or unmeasured technical factors, considering ECAD is a cell surface protein and robust changes were still observed in transcription factor markers. Comparison of response of these two cell types to paclitaxel revealed that the AXL-expressing “mesenchymal” AN3CA cells were more resistant to paclitaxel than were the AXL non-expressing “mesenchymal” AN3CA cells (Fig. 4F). Thus, we conclude that AXL is required for paclitaxel resistance independently of EMT.

4.8. AXL inhibition restores USC chemosensitivity in vivo

Finally, we wondered whether our *in vitro* findings regarding the role of AXL in chemoresistance would be recapitulated in an *in vivo* model. We subcutaneously injected ARK1shSCRM cells into NOD-SCID mice. After tumors had engrafted, we treated the mice with paclitaxel, BGB324, or paclitaxel plus BGB324 for 14 days. Measurement of tumor volume throughout this period revealed that the combination of paclitaxel plus BGB324 was significantly more effective at restricting tumor growth than was either drug alone (Fig. 5). In agreement with previous findings in our laboratory, AXL inhibition alone was not found to significantly decrease proliferation in xenograft models [6]. These results indicate that AXL inhibition enhances USC sensitivity to paclitaxel *in vivo*.

5. Discussion

Current drug regimens for USC are suboptimal, as evidenced by the fact that most patients relapse with and die as a result of chemotherapy-resistant disease [3, 42]. To improve outcomes for these patients requires defining the mechanisms by which USC becomes chemoresistant and developing strategies to restore chemosensitivity. We present here evidence that the receptor tyrosine kinase AXL participates in chemoresistance and is an attractive target for development of new treatment strategies. We show that AXL expression was highest in chemoresistant tumor samples from USC patients. Next, we demonstrate that AXL expression is required for paclitaxel resistance in USC cell lines and that inhibition of AXL with the small molecule BGB324 restores paclitaxel sensitivity *in vitro*. Finally, we

report that inhibition of AXL with BGB324 acts in an additive fashion with paclitaxel to reduce tumor burden in an *in vivo* xenograft model of USC. Combined with our previous observations that AXL was required for uterine cancer cell invasion and metastasis, and that AXL expression correlated with overall worse prognosis in uterine cancer patients [6], these findings provide strong preclinical support for combining an AXL inhibitor with paclitaxel in USC clinical trials.

This study also provides new evidence regarding three mechanisms by which AXL promotes resistance to paclitaxel. First, AXL expression limits USC cell accumulation of paclitaxel. Second, AXL-mediated chemoresistance is independent of the epithelial-mesenchymal transition. Third, AXL reduces paclitaxel-mediated cell cycle inhibition and apoptosis.

The first way in which AXL acts is by limiting accumulation of paclitaxel in USC cells. AXL has been implicated in chemoresistance in other cancers [16-19], but this is the first demonstration that AXL acts by limiting drug accumulation in USC cells. One mechanism by which cancers become resistant to taxanes and other conventional cytotoxic agents is via upregulation of the drug efflux pumps ATP-binding cassette (ABC) transporters such as ABCB1, ABCB2, and ABCC10 [43-47]. Additionally, intracellular paclitaxel accumulation is associated with increased expression of ABC transporters in multiple cell types [47-49]. Recently, Lin and colleagues showed that mRNA levels for the transport protein ABCB1 were upregulated in AXL-expressing docetaxel-resistant prostate cancer cells [25]. We also demonstrate a relationship between AXL expression and ABCB1 mRNA levels, where AXL inactivation in chemoresistant cells produced decreased ABCB1 transcript levels. Although our data suggest that AXL affects paclitaxel uptake or accumulation rather than efflux alone, future work will investigate the role of ABC transporters in paclitaxel resistance in USC.

The second novel finding regarding the mechanism by which AXL promotes paclitaxel resistance came from our assessment of the role of EMT, revealing, for the first time in any cancer, that AXL is required for chemoresistance independently of the epithelial or mesenchymal phenotype of the cells. For example, Lin and colleagues showed that inhibition of AXL reversed EMT in prostate cancer cells, but they did not assess whether chemosensitivity could be restored with AXL knockdown [25]. Similarly, several reports suggest that inhibition or knockdown of AXL reduces the resistance of mesenchymal cells to chemotherapeutic drugs while also reverting them to an epithelial state [18, 33, 38, 50, 51]. Our finding that inactivation of AXL improves chemosensitivity without affecting the mesenchymal phenotype indicates that AXL directly regulates chemoresistance.

The third way in which AXL acts is by reducing paclitaxel-mediated cell cycle arrest and apoptosis. Taxane therapy abrogates completion of mitosis by blocking cells in the G2/M phase of the cell cycle [41, 52-54], and AXL-expressing USC cells accumulate in this phase to a greater degree than AXL-non-expressing cells in the presence of paclitaxel. This G2/M arrest then leads to apoptotic cell death. These findings are consistent with the current literature on AXL mediated chemoresistance [16, 23-25, 53].

Our data provide preclinical *in vitro* and *in vivo* evidence that BGB324 (also called R428) [37] is a promising drug for treatment of USC. Although this drug has not been used

extensively in gynecologic cancers, preclinical data show success with BGB324 as monotherapy and in combination treatment in cancers such as acute myeloid leukemia (AML), non-small cell lung cancer (NSCLC), melanoma, breast, head and neck, esophageal, prostate, and endometrial [6, 16, 17, 25, 54-57]. Synergism between BGB324 and taxane therapy has been demonstrated in other tumor types [16, 25], and BGB324 is currently being investigated in several phase I/II trials. For example, BGB324 is being used in combination with docetaxel or with erlotinib for management of NSCLC, as monotherapy or in combination with cytarabine for management of acute myeloid leukemia, and in combination with pembrolizumab or dabrafenib and trametinib for management of melanoma. Phase I studies demonstrated safety of BGB324 at efficacious doses [58]. Our data indicate that AXL inhibitors should be tested in combination with paclitaxel in clinical trials for USC, especially for cases that have developed resistance to chemotherapy or other treatments.

Supplementary Material

Refer to Web version on PubMed Central for supplementary material.

Acknowledgments

The authors thank the Thomas Quinn and Susan Deutscher laboratories (Biochemistry Department, University of Missouri, Columbia, MO, USA) for assistance with [H^3]paclitaxel accumulation studies, Thomas Walsh for assistance with constructing the tumor microarray (Washington University St. Louis Breast Tissue Registry), and Dr. Deborah J. Frank for critical review of the manuscript.

Financial Support: Research reported in this publication was supported by NIH grant 2K12HD000849-28 (with co-funding from the American College of Obstetrics and Gynecologists and the March of Dimes) (K.C. Fuh), Cancer Frontier Fund grants 8002-88 and 3794 (K.C. Fuh), and American Cancer Society grant IRG-58-010-59-3 (K.C. Fuh).

References

1. Siegel RL, Miller KD, Jemal A. Cancer Statistics, 2017. CA Cancer J Clin. 2017; 67(1):7–30. [PubMed: 28055103]
2. Bokhman JV. Two pathogenetic types of endometrial carcinoma. Gynecol Oncol. 1983; 15(1):10–7. [PubMed: 6822361]
3. Boruta DM 2nd, et al. Management of women with uterine papillary serous cancer: a Society of Gynecologic Oncology (SGO) review. Gynecol Oncol. 2009; 115(1):142–53. [PubMed: 19592079]
4. Fleming GF, et al. Phase III trial of doxorubicin plus cisplatin with or without paclitaxel plus filgrastim in advanced endometrial carcinoma: a Gynecologic Oncology Group Study. J Clin Oncol. 2004; 22(11):2159–66. [PubMed: 15169803]
5. Colombo N, et al. ESMO-ESGO-ESTRO Consensus Conference on Endometrial Cancer: Diagnosis, Treatment and Follow-up. Int J Gynecol Cancer. 2016; 26(1):2–30. [PubMed: 26645990]
6. Divine LM, et al. AXL modulates extracellular matrix protein expression and is essential for invasion and metastasis in endometrial cancer. Oncotarget. 2016; 7(47):77291–77305. [PubMed: 27764792]
7. Paccez JD, et al. The receptor tyrosine kinase Axl is an essential regulator of prostate cancer proliferation and tumor growth and represents a new therapeutic target. Oncogene. 2013; 32(6):689–98. [PubMed: 22410775]
8. Paccez JD, et al. Inactivation of GSK3beta and activation of NF-kappaB pathway via Axl represents an important mediator of tumorigenesis in esophageal squamous cell carcinoma. Mol Biol Cell. 2015; 26(5):821–31. [PubMed: 25568334]

9. Rankin EB, et al. AXL is an essential factor and therapeutic target for metastatic ovarian cancer. Cancer Res. 2010; 70(19):7570–9. [PubMed: 20858715]
10. Sun WS, Fujimoto J, Tamaya T. Coexpression of growth arrest-specific gene 6 and receptor tyrosine kinases Axl and Sky in human uterine endometrial cancers. Ann Oncol. 2003; 14(6):898–906. [PubMed: 12796028]
11. Sun W, Fujimoto J, Tamaya T. Coexpression of Gas6/Axl in human ovarian cancers. Oncology. 2004; 66(6):450–7. [PubMed: 15452374]
12. Pinato DJ, Chowdhury S, Stebbing J. TAMing resistance to multi-targeted kinase inhibitors through Axl and Met inhibition. Oncogene. 2016; 35(21):2684–6. [PubMed: 26434595]
13. Chen QY, et al. Silencing of Rac1 modifies lung cancer cell migration, invasion and actin cytoskeleton rearrangements and enhances chemosensitivity to antitumor drugs. Int J Mol Med. 2011; 28(5):769–76. [PubMed: 21837360]
14. Linger RM, et al. TAM receptor tyrosine kinases: biologic functions, signaling, and potential therapeutic targeting in human cancer. Adv Cancer Res. 2008; 100:35–83. [PubMed: 18620092]
15. Braunger J, et al. Intracellular signaling of the Ufo/Axl receptor tyrosine kinase is mediated mainly by a multi-substrate docking-site. Oncogene. 1997; 14(22):2619–31. [PubMed: 9178760]
16. Wilson C, et al. AXL inhibition sensitizes mesenchymal cancer cells to antimitotic drugs. Cancer Res. 2014; 74(20):5878–90. [PubMed: 25125659]
17. Giles KM, et al. Axl mediates acquired resistance of head and neck cancer cells to the epidermal growth factor receptor inhibitor erlotinib. Mol Cancer Ther. 2013; 12(11):2541–58. [PubMed: 24026012]
18. Byers LA, et al. An epithelial-mesenchymal transition gene signature predicts resistance to EGFR and PI3K inhibitors and identifies Axl as a therapeutic target for overcoming EGFR inhibitor resistance. Clin Cancer Res. 2013; 19(1):279–90. [PubMed: 23091115]
19. Zhang Z, et al. Activation of the AXL kinase causes resistance to EGFR-targeted therapy in lung cancer. Nat Genet. 2012; 44(8):852–60. [PubMed: 22751098]
20. Elkabets M, et al. AXL mediates resistance to PI3Kα inhibition by activating the EGFR/PKC/mTOR axis in head and neck and esophageal squamous cell carcinomas. Cancer Cell. 2015; 27(4):533–46. [PubMed: 25873175]
21. Meyer AS, et al. The receptor AXL diversifies EGFR signaling and limits the response to EGFR-targeted inhibitors in triple-negative breast cancer cells. Sci Signal. 2013; 6(287):ra66. [PubMed: 23921085]
22. Antony J, et al. The GAS6-AXL signaling network is a mesenchymal (Mes) molecular subtype-specific therapeutic target for ovarian cancer. Sci Signal. 2016; 9(448):ra97. [PubMed: 27703030]
23. Keating AK, et al. Inhibition of Mer and Axl receptor tyrosine kinases in astrocytoma cells leads to increased apoptosis and improved chemosensitivity. Mol Cancer Ther. 2010; 9(5):1298–307. [PubMed: 20423999]
24. Li Y, et al. Inhibition of Mer and Axl receptor tyrosine kinases leads to increased apoptosis and improved chemosensitivity in human neuroblastoma. Biochem Biophys Res Commun. 2015; 457(3):461–6. [PubMed: 25596315]
25. Lin JZ, et al. Targeting AXL overcomes resistance to docetaxel therapy in advanced prostate cancer. Oncotarget. 2017
26. Gausdal G. Abstract 566: BGB324, a selective small molecule inhibitor of the recetor tyrosine kinase AXL, enhances immune checkpoint inhibitor efficacy. Cancer Res. 2016 e.a.
27. Gjerdrum C, et al. Axl is an essential epithelial-to-mesenchymal transition-induced regulator of breast cancer metastasis and patient survival. Proc Natl Acad Sci U S A. 2010; 107(3):1124–9. [PubMed: 20080645]
28. Schoumacher M, Burbridge M. Key Roles of AXL and MER Receptor Tyrosine Kinases in Resistance to Multiple Anticancer Therapies. Curr Oncol Rep. 2017; 19(3):19. [PubMed: 28251492]
29. Asiedu MK, et al. AXL induces epithelial-to-mesenchymal transition and regulates the function of breast cancer stem cells. Oncogene. 2014; 33(10):1316–24. [PubMed: 23474758]

30. Del Pozo Martin Y, et al. Mesenchymal Cancer Cell-Stroma Crosstalk Promotes Niche Activation, Epithelial Reversion, and Metastatic Colonization. Cell Rep. 2015; 13(11):2456–69. [PubMed: 26670048]
31. Wang C, et al. Gas6/Axl Axis Contributes to Chemoresistance and Metastasis in Breast Cancer through Akt/GSK-3beta/beta-catenin Signaling. Theranostics. 2016; 6(8):1205–19. [PubMed: 27279912]
32. Gao J, et al. Integrative Analysis of Complex Cancer Genomics and Clinical Profiles Using the cBioPortal. Science Signalling. 2013; 6(269)
33. Cerami E, et al. The cBio cancer genomics portal: an open platform for exploring multidimensional cancer genomics data. Cancer Discov. 2012; 2(5):401–4. [PubMed: 22588877]
34. Hendricks DT, et al. FHIT Gene Expression in Human Ovarian, Endometrial, and Cervical Cancer Cell Lines. Cancer Res. 1997; 57:2112–2115. [PubMed: 9187105]
35. El-Sahwi K, et al. In vitro activity of pertuzumab in combination with trastuzumab in uterine serous papillary adenocarcinoma. Br J Cancer. 2010; 102(1):134–43. [PubMed: 19920829]
36. Holland SJ, et al. Multiple roles for the receptor tyrosine kinase axl in tumor formation. Cancer Res. 2005; 65(20):9294–303. [PubMed: 16230391]
37. Heinrich MC, et al. Inhibition of c-kit receptor tyrosine kinase activity by STI 571, a selective tyrosine kinase inhibitor. Blood. 2000; 96(3):925–32. [PubMed: 10910906]
38. Pinzon-Daza ML, et al. Oxidative Stress Promotes Doxorubicin-Induced Pgp and BCRP Expression in Colon Cancer Cells Under Hypoxic Conditions. J Cell Biochem. 2017; 118(7): 1868–1878. [PubMed: 28106284]
39. Rankin EB, et al. Direct regulation of GAS6/AXL signaling by HIF promotes renal metastasis through SRC and MET. Proc Natl Acad Sci U S A. 2014; 111(37):13373–8. [PubMed: 25187556]
40. Cancer Genome Atlas Research, N. et al. Integrated genomic characterization of endometrial carcinoma. Nature. 2013; 497(7447):67–73. [PubMed: 23636398]
41. Horwitz SB. Taxol (paclitaxel): mechanisms of action. Ann Oncol. 1994; 5(Suppl 6):S3–6.
42. Moore KN, Fader AN. Uterine papillary serous carcinoma. Clin Obstet Gynecol. 2011; 54(2):278–91. [PubMed: 21508697]
43. Yusuf RZ, et al. Paclitaxel resistance: molecular mechanisms and pharmacologic manipulation. Curr Cancer Drug Targets. 2003; 3(1):1–19. [PubMed: 12570657]
44. Tian C, et al. Common variants in ABCB1, ABCC2 and ABCG2 genes and clinical outcomes among women with advanced stage ovarian cancer treated with platinum and taxane-based chemotherapy: a Gynecologic Oncology Group study. Gynecol Oncol. 2012; 124(3):575–81. [PubMed: 22112610]
45. Vergara D, et al. Lapatinib/Paclitaxel polyelectrolyte nanocapsules for overcoming multidrug resistance in ovarian cancer. Nanomedicine. 2012; 8(6):891–9.
46. Barbuti AM, Chen ZS. Paclitaxel Through the Ages of Anticancer Therapy: Exploring Its Role in Chemoresistance and Radiation Therapy. Cancers (Basel). 2015; 7(4):2360–71. [PubMed: 26633515]
47. Kathawala RJ, et al. Masitinib antagonizes ATP-binding cassette subfamily C member 10-mediated paclitaxel resistance: a preclinical study. Mol Cancer Ther. 2014; 13(3):714–23. [PubMed: 24431074]
48. Wang YJ, et al. Regorafenib overcomes chemotherapeutic multidrug resistance mediated by ABCB1 transporter in colorectal cancer: In vitro and in vivo study. Cancer Lett. 2017; 396:145–154. [PubMed: 28302530]
49. Wang YJ, et al. Thiazole-valine peptidomimetic (TTT-28) antagonizes multidrug resistance in vitro and in vivo by selectively inhibiting the efflux activity of ABCB1. Sci Rep. 2017; 7:42106. [PubMed: 28181548]
50. Linger RM, et al. Mer or Axl receptor tyrosine kinase inhibition promotes apoptosis, blocks growth and enhances chemosensitivity of human non-small cell lung cancer. Oncogene. 2013; 32(29): 3420–31. [PubMed: 22890323]
51. Fleuren ED, et al. The role of AXL and the in vitro activity of the receptor tyrosine kinase inhibitor BGB324 in Ewing sarcoma. Oncotarget. 2014; 5(24):12753–68. [PubMed: 25528764]

52. Tuck C, et al. Robust mitotic entry is ensured by a latching switch. Biol Open. 2013; 2(9):924–31. [PubMed: 24143279]

53. Potapova TA, et al. Fine tuning the cell cycle: activation of the Cdk1 inhibitory phosphorylation pathway during mitotic exit. Mol Biol Cell. 2009; 20(6):1737–48. [PubMed: 19158392]

54. Sakurikar N, Eichhorn JM, Chambers TC. Cyclin-dependent kinase-1 (Cdk1)/cyclin B1 dictates cell fate after mitotic arrest via phosphoregulation of antiapoptotic Bcl-2 proteins. J Biol Chem. 2012; 287(46):39193–204. [PubMed: 22965228]

55. Brand TM, et al. AXL Is a Logical Molecular Target in Head and Neck Squamous Cell Carcinoma. Clin Cancer Res. 2015; 21(11):2601–12. [PubMed: 25767293]

56. Hector A, et al. The Axl receptor tyrosine kinase is an adverse prognostic factor and a therapeutic target in esophageal adenocarcinoma. Cancer Biol Ther. 2010; 10(10):1009–18. [PubMed: 20818175]

57. Holland SJ, et al. R428, a selective small molecule inhibitor of Axl kinase, blocks tumor spread and prolongs survival in models of metastatic breast cancer. Cancer Res. 2010; 70(4):1544–54. [PubMed: 20145120]

58. Loges S. A first-in-patient phase I study of BGB324, a selective Axl kinase inhibitor in patients with refractory/relapsed AML and high-risk MDS. ASCO. 2016

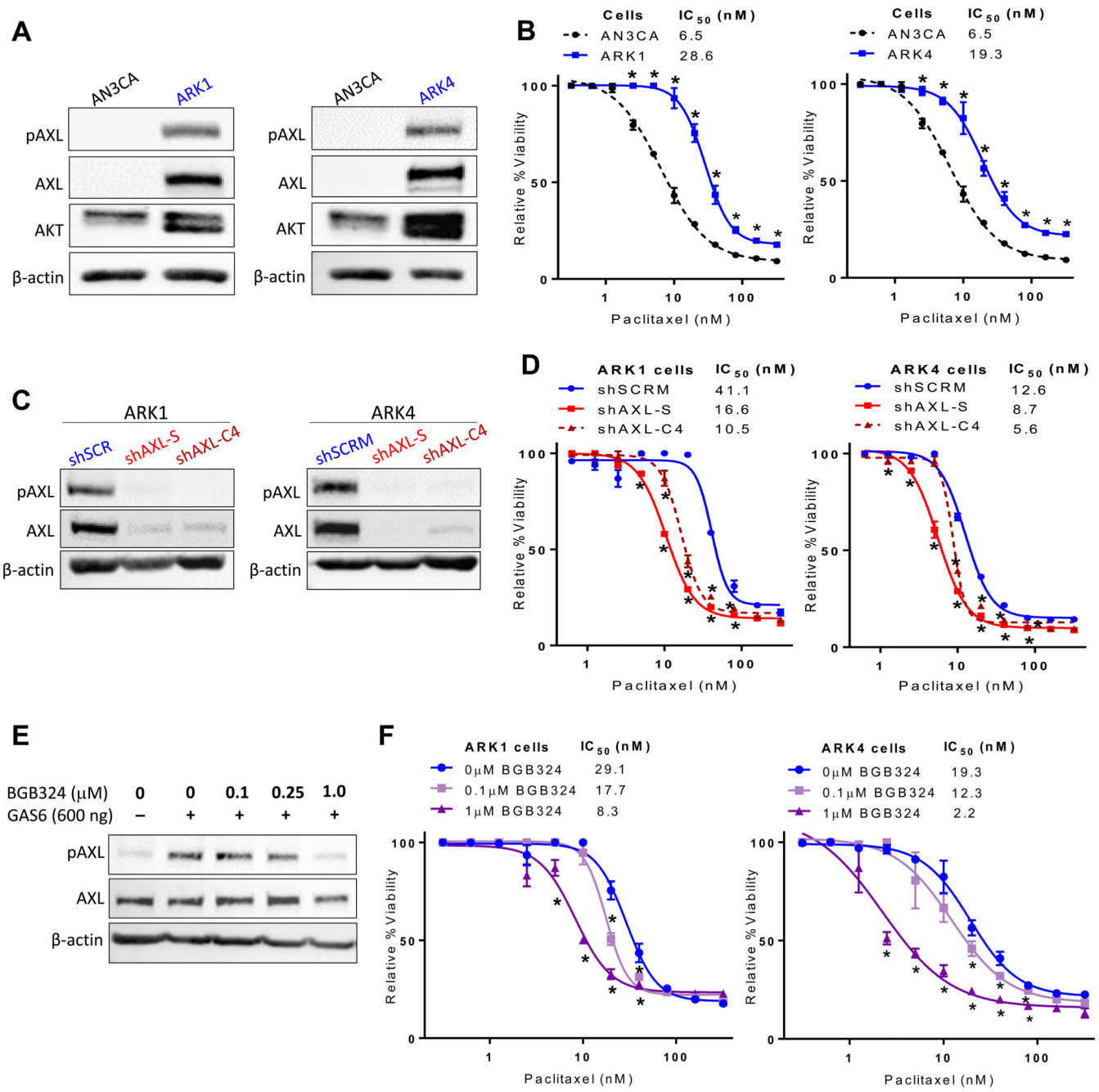

Figure 1. AXL expression is elevated in paclitaxel resistant USC cell lines, and AXL inhibition restores chemosensitivity

(A) Western blot detection of AXL in AN3CA, ARK1, and ARK4 cells with β-actin used as a loading control. **(B)** Results of XTT assay of cell viability in increasing concentrations of paclitaxel. **(C)** Western blot detection of AXL in lysates of ARK1 and ARK4 cells transfected with the indicated shRNAs. shAXL-S and shAXL-C4 target AXL, and shSCRM is nonspecific. **(D)** Results of XTT assay of cell viability in increasing concentrations of paclitaxel. **(E)** Western blot detection of AXL and phosphorylated AXL (pAXL) in ARK1 cells treated with the AXL inhibitor BGB324. **(F)** Results of XTT assay of cell viability in

increasing concentrations of paclitaxel and the indicated concentrations of BGB324. In **(B)**, **(D)**, and **(F)**, cell viability is expressed relative to the respective controls treated with vehicle (DMSO). XTT assays were performed in triplicate and graphed as the mean ± SD. **P*< 0.05 compared to matched controls.

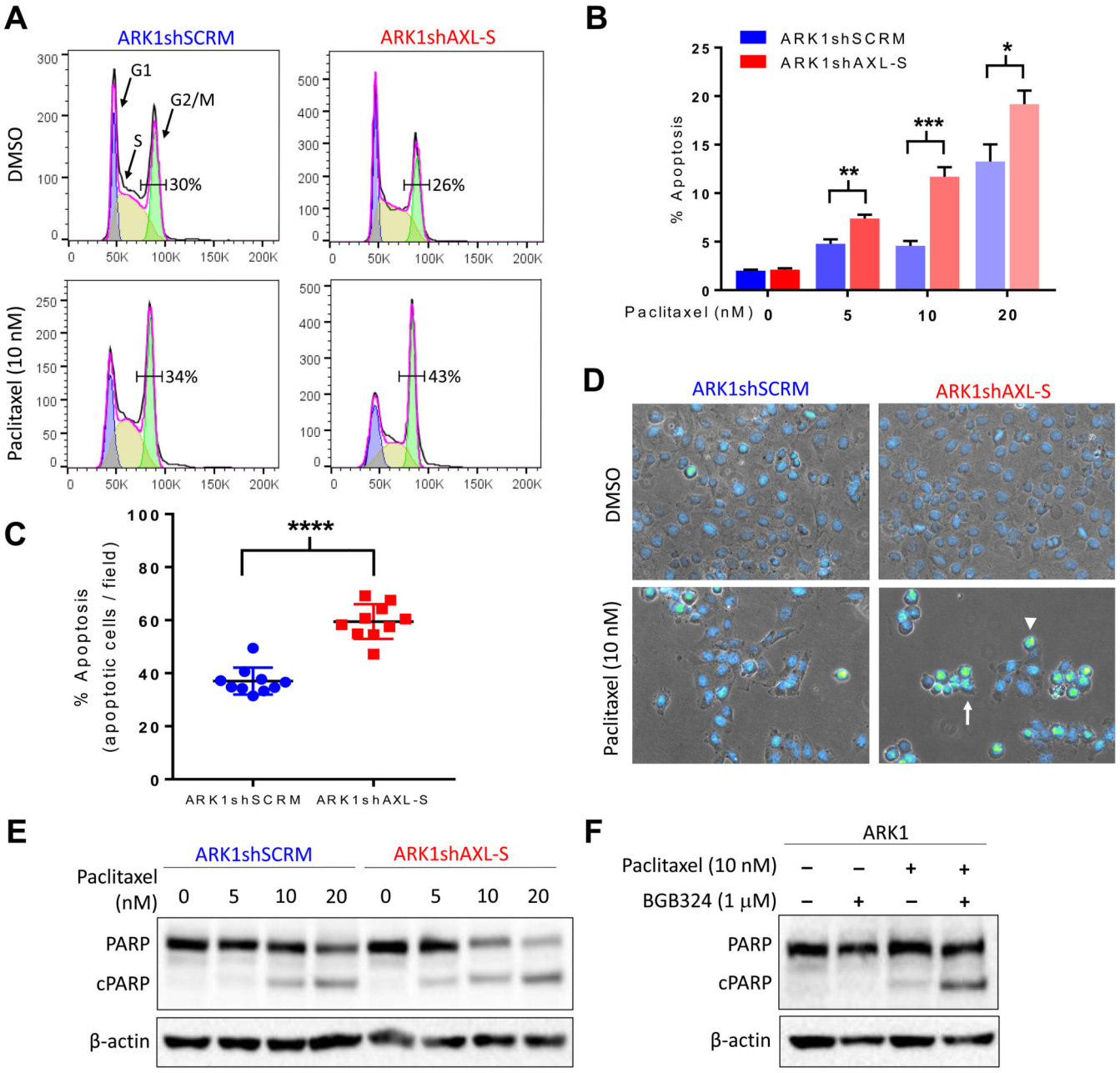

Figure 2. AXL knockdown or inhibition increases paclitaxel-mediated apoptosis

(A) Flow cytometry analysis of cell cycle distribution in ARK1shSCRM and ARK1shAXL-S cells treated with paclitaxel or vehicle (DMSO). Numbers indicate the percentage of cells in G2/M. **(B)** Percentage of paclitaxel-treated ARK1shSCRM and ARK1shAXL-S cells detected as apoptotic in the Annexin-V/PI assay. Values are reported as the mean ± SD. **P*< 0.05 ***P*< 0.01, ****P*< 0.001. **(C)** and **(D)** Quantitation (**C**) and representative images (**D**) of apoptotic ARK1shSCRM and ARK1shAXL-S cells detected by staining with DAPI and microscopic analysis of nuclear morphology. Arrow indicates blebbing, arrowhead indicates abnormal DNA condensation. *****P*< 0.0001. **(E and F)** Western blot detection of full-length and cleaved PARP in **(E)** ARK1shSCRM and ARK1shAXL-S cells treated with

increasing doses of paclitaxel and **(F)** ARK1 cells treated with vehicle, paclitaxel, BGB324, or paclitaxel plus BGB324.

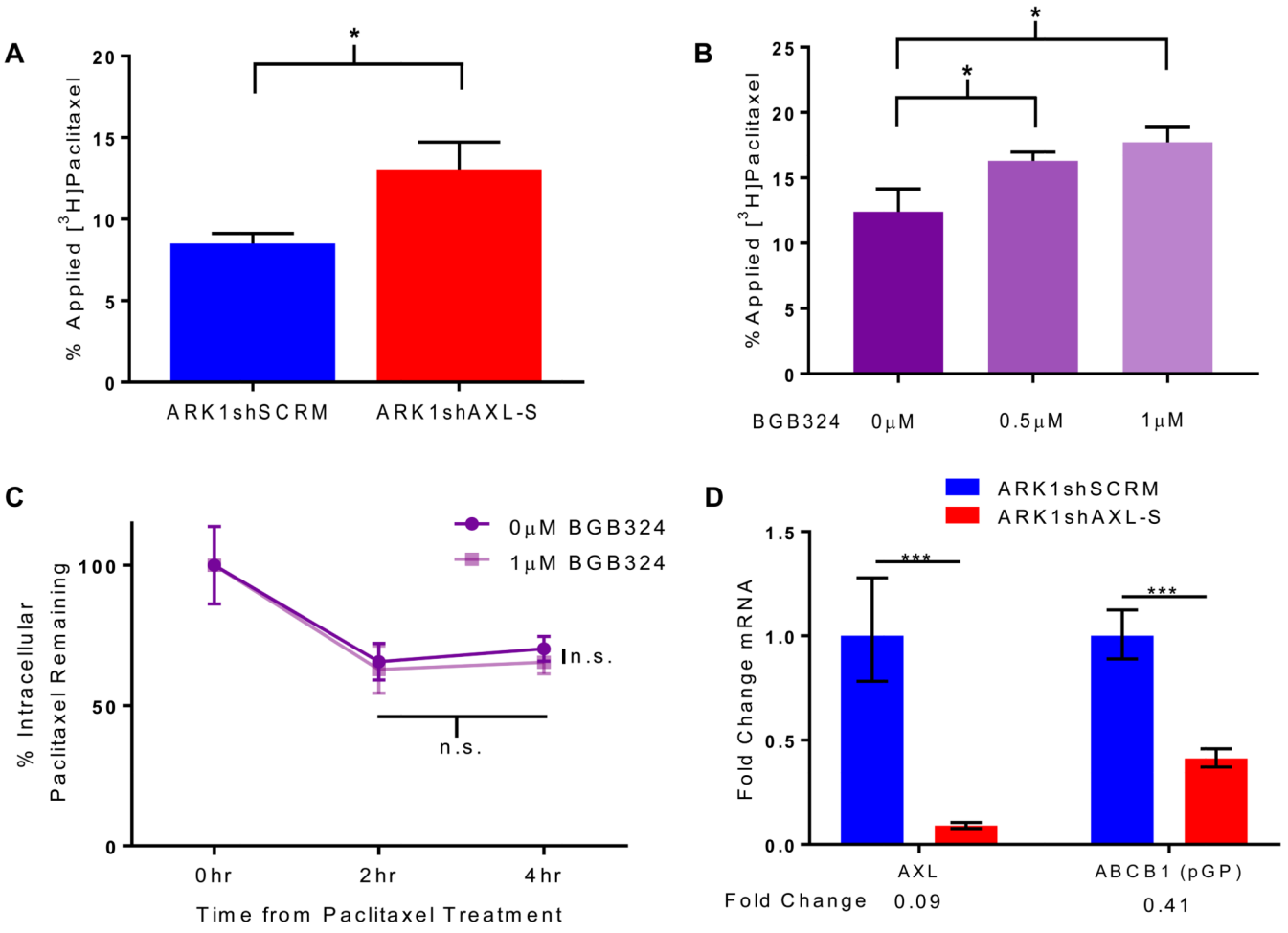

Figure 3. AXL knockdown or inhibition increases intracellular paclitaxel accumulation

(A) Quantitation of intracellular [^{3}H]paclitaxel in ARK1shSCRM-S and ARK1shAXL-S cells. **(B)** Quantitation of intracellular [^{3}H]paclitaxel in ARK1 cells treated with vehicle or the AXL inhibitor BGB324. **(C)** Quantitation of [^{3}H]paclitaxel in ARK1 cells after a two-hour washout period. **(D)** qPCR was performed on ARK1 cells transfected with shSCRM or shAXL-S, and expression patterns of mRNA were assessed. Error bars indicate range of the fold change, and significance was calculated using SD of DDC_T. *P< 0.05, ***P< 0.001.

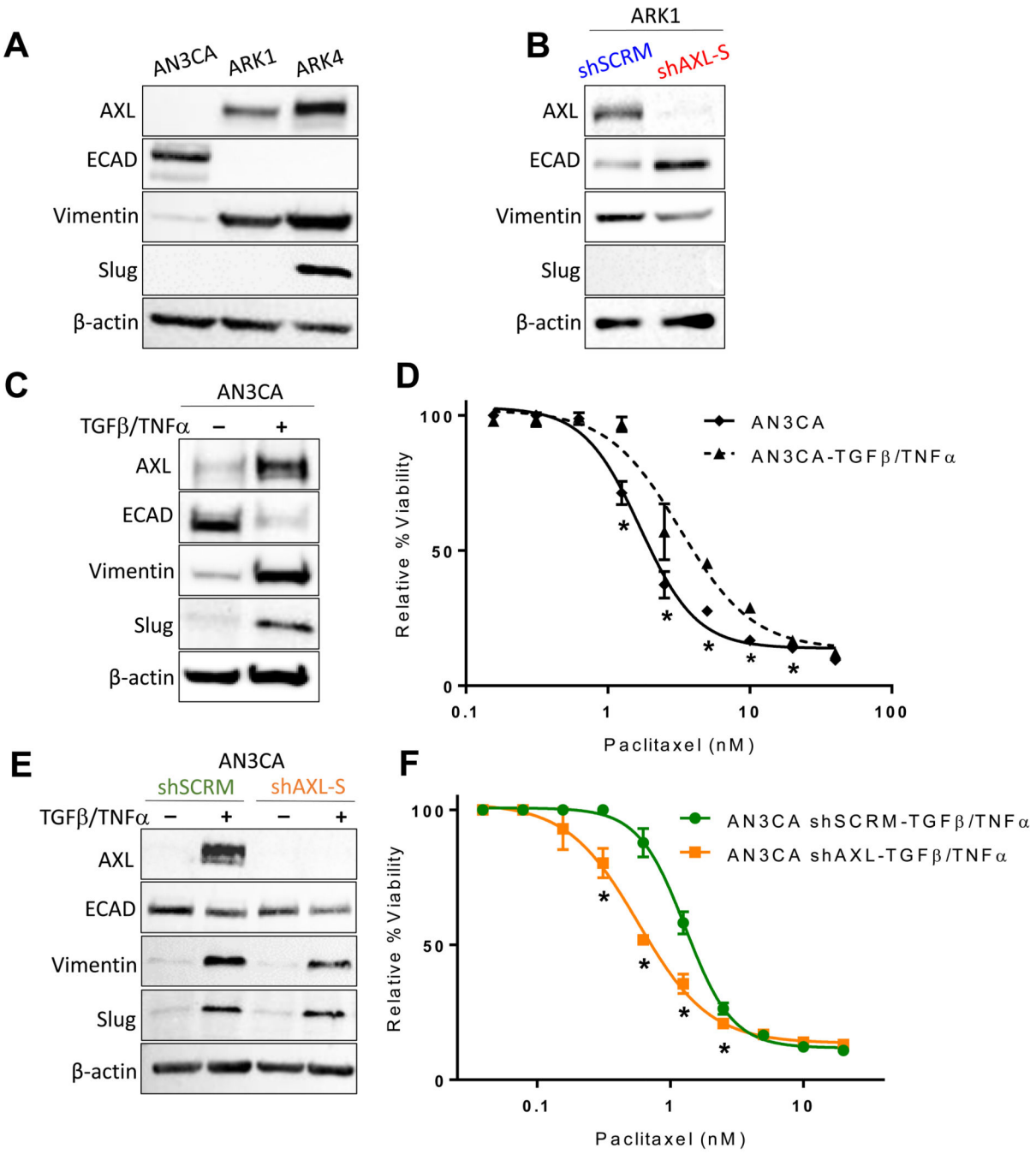

Figure 4. AXL-mediated paclitaxel resistance is independent of the epithelial-to-mesenchymal transition

(A, B, C, E) Western blot detection of AXL and mesenchymal and epithelial markers, plus β-actin as a loading control, in **(A)** AN3CA, ARK1, and ARK4 cells, **(B)** ARK1 cells transfected with shAXL-S or shSCRM, **(C)** AN3CA cells treated with 100 ng TGFβ and 50 ng TNFα to induce EMT, and **(E)** AN3CA cells transfected with shAXL-S or shSCRM. **(D and F)** Results of XTT assays of cell viability in increasing concentrations of paclitaxel of **(D)** AN3CA cells treated with or without TGFβ and TNFα to induce EMT and **(F)**

AN3CAshSCRM and AN3CAshAXL-S cells that had undergone TGFβ-induced EMT. XTT assays were performed in triplicate and graphed as the mean ± SD. *$P < 0.05$ compared to matched control.

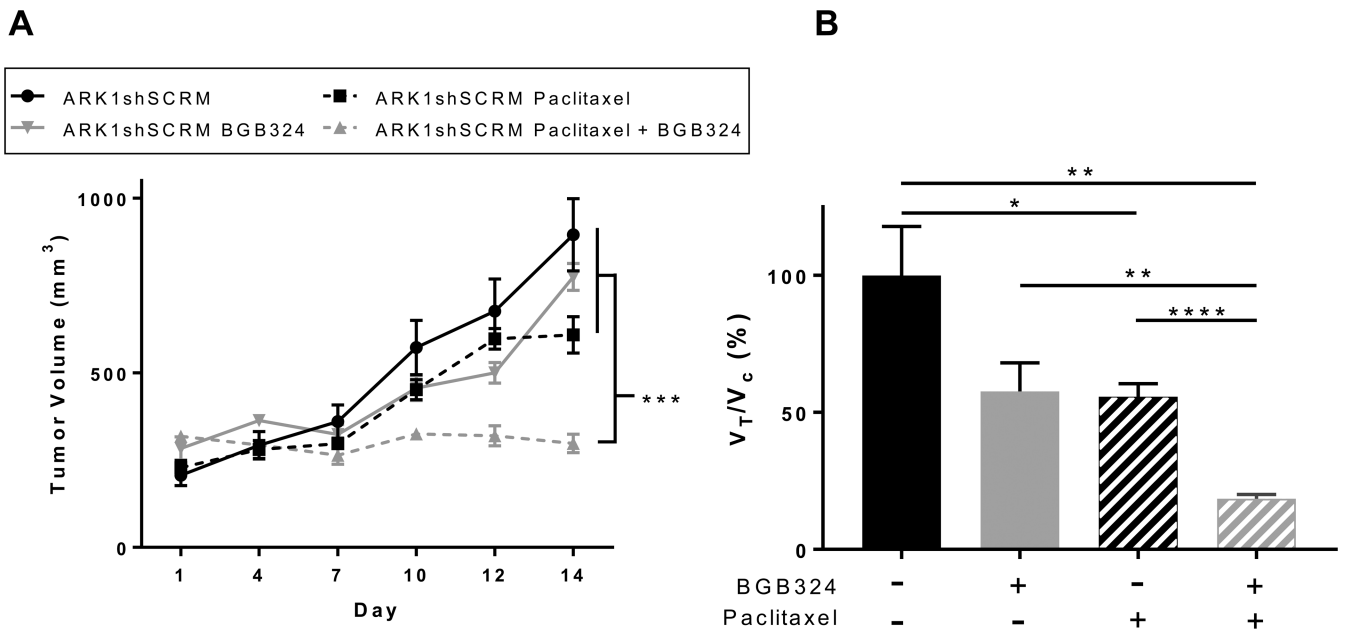

Figure 5. AXL inhibition improves chemoresponse in subcutaneous xenograft tumors *in vivo*

(A) Volume of tumors over 14 days in mice injected with ARK1shSCRM cells and treated with vehicle, paclitaxel, BGB324, or paclitaxel plus BGB324. Mean tumor volume (n=6 per group) and S.E. are plotted. ****P*< 0.001 by one-way ANOVA of tumor volume data collected on day 14. **B)** Quantitation of relative tumor proliferation rate ($V_{Treatment}/V_{Control}$) calculated by using the tumor volumes at day 14 relative to tumor volumes at initial treatment administration. **P*< 0.05, ***P*< 0.01, ****P*< 0.001, *****P*< 0.0001.

Table 1

Associations between AXL expression and chemoresponse in 82 USC patient tumors

	AXL H-score	Score Distribution (n)			
Chemoresponse	**Mean Score**	**3 (100%-71%)**	**2 (70%-41%)**	**1 (40%-16%)**	**0 (15%-0%)**
No Recurrence	1.8	6	13	7	3
Chemosensitive	1.6	4	11	10	2
Chemoresistant	2.3 *	13	9	4	0

* The asterisk indicates significant difference in AXL histology score from chemoresistant and no recurrence / chemosensitive (*$P < 0.05$).